Journal of
Materials Chemistry A

Materials for energy and sustainability

Accepted Manuscript

This article can be cited before page numbers have been issued, to do this please use: L. Sun, Z. Shi, H. Wang, K. Zhang, D. Davoud, K. Sun and R. Fan, *J. Mater. Chem. A*, 2020, DOI: 10.1039/D0TA00903B.

ROYAL SOCIETY OF CHEMISTRY

rsc.li/materials-a

View Article Online
DOI: 10.1039/D0TA00903B

Ultrahigh Discharge Efficiency and Improved Energy Density in Rationally Designed Bilayer Polyetherimide-$BaTiO_3$/P(VDF-HFP) Composites

Liang Sun[a], Zhicheng Shi[a,*], Huanlei Wang[a], Kun Zhang[b,*], Davoud Dastan[c], Kai Sun [d], Runhua Fan[d]

[a]School of Materials Science and Engineering, Ocean University of China, Qingdao 266100, P. R. China

[b]Key Laboratory of Microgravity (National Microgravity Laboratory), Institute of Mechanics, Chinese Academy of Sciences, Beijing 100190, China

[c]Department of Materials Science and Engineering, Georgia Institute of Technology, Atlanta, Georgia-30332, USA

[d]Institute of Marine Materials Science and Engineering, Shanghai Maritime University, Shanghai 201306, P. R. China

[*]Corresponding author: Zhicheng Shi, Kun Zhang

[*]E-mail: zcshi@ouc.edu.cn, zhangkun@imech.ac.cn

View Article Online
DOI: 10.1039/D0TA00903B

Abstract

Polymer dielectric composites are of great interest for film capacitors that are widely used in pulsed power systems. For a long time, huge efforts have been devoted to achieving energy densities as high as possible to satisfy the miniaturization and high integration of electronic devices. However, the discharge efficiency which is particularly crucial to practical applications gained little attention. With the target of achieving concurrently improved energy density and efficiency, a class of rationally designed bilayer composites consisting of a pure polyetherimide layer and a $BaTiO_3$/P(VDF-HFP) composite layer were prepared. Interestingly, the bilayer composites exhibit ultrahigh discharge efficiencies η (> 95 %) under external electric fields up to 400 kV/mm which are much higher than most of the so far reported results (η < 80 %). Meanwhile, low loss (tanδ < 0.05 @10 kHz) that are comparable to the pure polyetherimide are obtained. In addition, the bilayer composites show impressive improvements in breakdown strengths E_b, i.e., 285 %, 363 %, 366 % and 567% for composites with 5 vol%, 10 vol%, 20 vol% and 40 vol% $BaTiO_3$, compared to their single layer counterparts, thus results in obviously improved energy densities U_e. In particular, the bilayer composite with 10 vol% $BaTiO_3$ displays the most prominent comprehensive energy storage performance, i.e., η ~ 96.8 % @450 kV/mm, U_e ~ 6

View Article Online
DOI: 10.1039/D0TA00903B

J/cm^3 @450 kV/mm, tanδ ~ 0.025 @10 kHz, E_b ~ 483.18 kV/mm. The ultrahigh discharged efficiencies and high energy densities, along with low loss and breakdown strengths make these bilayer composites ideal candidates for high-performance dielectric energy-storage capacitors.

Key words: dielectric permittivity, polymer composite, discharged efficiency, bilayer structure, film capacitor

1. Introduction

Polymer film capacitors (PFCs) have drawn considerable attention in recent years owing to their superior charge-discharge capabilities, outstanding cycling stabilities, excellent self-healing capability and wide applications in hybrid electric vehicles, medical defibrillator, and electromagnetic launch systems, etc.[1-4] However, the applications of the PFCs are greatly restricted by their low energy densities. In principle, the energy density (U_d) of a dielectric material can be expressed as equations: $U_d = 1/2\varepsilon_0\varepsilon_r E^2$ for a linear dielectric material and $U_d = \int E\mathrm{d}D$ for a nonlinear dielectric material, where ε_0 and ε_r represent the dielectric permittivities of the vacuum and dielectrics, E is the applied electric field which should be lower than the breakdown strength (E_b) of the materials, and $D = \varepsilon_0\varepsilon_r E$ is electric displacement. Accordingly, high ε_r and high E_b are desired for high U_d. To achieve this, various strategies have been proposed, among which constructing polymer based composites filled with high ε_r or high E_b fillers has been demonstrated to be effective.[5-7] To obtain improved ε_r, ferroelectric ceramic fillers

DOI: 10.1039/D0TA00903B

(e.g., $BaTiO_3$,[8,9] $SrTiO_3$,[10] $NaNbO_3$,[11] etc.) and conductors (e.g., metals,[12-14] carbon nanotubes,[15] graphene,[16,17] conductive polymers,[18] etc.) are usually employed. However, improved ε_r is always accompanied with suppressed E_b, deteriorated η and elevated loss.[19] To achieve improved E_b, fillers with high E_b (e.g., boron nitride, alumina, silica, etc.) are usually employed as the fillers.[1,2] Unfortunately, the fillers with high E_b often exhibit low ε_r, leading to suppressed ε_r.[20] As a result, the reasonable balance between ε_r and E_b is until now a problem demanding prompt solution. Although various innovative strategies, such as designing core-shell structured fillers,[21,22] surface modification of fillers,[23-25] have been proposed to address this dilemma, the effect is still not satisfactory.

Recently, researchers found that multilayer structured composites may offer a feasible paradigm to realize the concurrent improvement of ε_r and E_b.[26-29] Compared with single-layer composites, multilayer composites possess another type of mesoscopic interface between adjacent layers, in addition to the microscopic interfaces between the filler and matrix, which may induce strong interfacial polarization and extra charge storage.[30-32] Wang and co-workers reported a design of trilayered films consisting of stacked barium titanate/poly(vinylidene fluoride-co-hexafluoropropylene) ($BaTiO_3$/P(VDF-HFP)) nanocomposite layers, where the middle layer with high $BaTiO_3$ content offer high ε_r while the two outer layers with low $BaTiO_3$ content provide high E_b. A significantly improved E_b of ~ 526 kV/mm and a moderately enhanced ε_r of ~ 12 @1 kHz, in comparison with pure P(VDF-HFP) (E_b = 410 kV/mm, ε_r = 10 @1 kHz), are realized via controlling the $BaTiO_3$ content. Consequently, an ultrahigh discharged energy density of 26.4 J cm^{-3} and a superior discharged efficiency

View Article Online
DOI: 10.1039/D0TA00903B

of 72 % are obtained.[33] In addition to the typical trilayered composites, much attention has also been paid to multilayer composites with more than three layers. Jiang and co-workers[27] designed a series of multilayer $BaTiO_3$/P(VDF-HFP) composites with different number of layers. It is shown that, the composite with 16 layers exhibits a substantially improved E_b (~ 862.5 kV/mm) and an obviously enhanced ε_r (~ 16 @1 kHz) compared with pure P(VDF-HFP) (E_b = 600 kV/mm, ε_r = 10 @1 kHz). Therefore, an ultrahigh energy density of ~ 30.15 J/cm^3 and a high discharge efficiency of ~ 78 % are achieved simultaneously.

Up to now, numerous multilayer composites with rationally designed hierarchical structures have been developed.[33-37] However, most of the reported results aimed at achieving energy densities as high as possible and thus choosing nonlinear ferroelectric polymer poly(vinylidene fluoride) and its copolymers as the matrix. Although greatly improved energy densities have been obtained, it inevitably results in the suppressed discharge efficiency (η < 80 %) and elevated loss (tanδ > 0.1 @1 kHz), which can not meet the requirements in practical applications. In other words, more attention should be paid to the concurrent improvement of U_d and η rather than solely high U_d. As we know, linear dielectric polymers (e.g., polyetherimide, polypropylene, polyimide, polymethyl methacrylate) have very high η (> 95 %) and low loss (tanδ < 0.05 @1 kHz).[2,19] With the aim of achieving balanced energy density and discharge efficiency, we herein report a novel design of bilayer dielectric composites consisting of a pure polyetherimide (PEI) layer and a $BaTiO_3$/P(VDF-HFP) composite layer. In comparison with a trilayer composite which has two layer/layer interfaces, a bilayer composite

View Article Online
DOI: 10.1039/D0TA00903B

possesses only one layer/layer interface. Therefore, the loss induced by the interfacial polarization at the interfaces between adjacent layers could be suppressed in the bilayer composite, which is favorable for the achievement of high efficiency and low loss. As shown in Figure 1, the linear dielectric layer PEI offers high efficiency η, low loss, and high breakdown strength $E_{b,}$ while the nonlinear dielectric layer $BaTiO_3$/P(VDF-HFP) composite layer provides high energy density U_d. Consequently, the bilayer composites may combine the superiorities of the two layers, yielding simultaneous high η, high U_d , high E_b, and low loss. Interestingly, our results show that all of the bilayer composites exhibit ultrahigh η over 95 % which are much higher than most of the so far reported polymer dielectric composites (η < 80 %) under external electric fields up to 400 kV/mm. Moreover, low loss ($\tan\delta$ < 0.05 @10 kHz) that is comparable to the pure PEI are also achieved. Furthermore, the bilayer composites show impressive improvements in E_b, i.e., 285 %, 363%, 366 % and 567% for composites with 5 vol%, 10 vol%, 20 vol% and 40 vol% $BaTiO_3$, compared to their single-layer counterparts, thus results in obviously improved U_d. The outstanding dielectric characteristics make these bilayer composites promising candidates for high-performance energy-storage capacitors.

2. Experimental

2.1. Materials

Barium titanate ($BaTiO_3$, < 3 μm, > 99.5 %, Aladdin Industrial Corporation), poly (vinylidene fluoride-hexafluoropropylene) (P(VDF-HFP), 15 % HFP, PolyK Technologies, USA), polyetherimide (PEI, PolyK Technologies, USA), 1-Methyl-2-

View Article Online
DOI: 10.1039/D0TA00903B

pyrrolidone (C_5H_9NO, ≥ 99.0 % Sinopharm Chemical Reagent Co., Ltd.), sodium dodecylbenzenesulfonate ($C_{18}H_{29}NaO_3$, ≥ 88.0 %, Sinopharm Chemical Reagent Co., Ltd.) and ethanol (≥ 99.7 %, Sinopharm Chemical Reagent Co., Ltd.).

2.2. Preparation of bilayer composites

Firstly, $BaTiO_3$/P(VDF-HFP) suspension and PEI solution were prepared. For the preparation of $BaTiO_3$/P(VDF-HFP) suspension, $BaTiO_3$ particles and sodium dodecylbenzenesulfonate (SDBS) were ultrasonically dispersed into 10 mL 1-Methyl-2-pyrrolidone (NMP) for 1 h at room temperature to obtain a stable suspension, followed by adding P(VDF-HFP) pellets into the suspension with magnetic stirring at 75 °C until P(VDF-HFP) pellets were dissolved completely. For the preparation of PEI solution, PEI particles were directly dissolved into 1-Methyl-2-pyrrolidone (NMP) with rapid magnetic stirring at 75 °C for 5 h and mild stirring at room temperature overnight. Then the $BaTiO_3$/P(VDF-HFP) suspension and PEI solution were casted on glass plates respectively. The thicknesses of the single-layer composites were controlled in the range of 15-20 μm by adjusting the height of blade. Then the films along with the glass platers were transferred into in an oven and dried at 100 °C for 4 h and 200 °C for 5 min. subsequently, the films were peeled off via quenching in ice water and dried in an oven at 70 °C for 6 h, yielding the single layer $BaTiO_3$/P(VDF-HFP) composite films and PEI films. Finally, bilayer films with different $BaTiO_3$ contents were obtained via stacking and hot-pressing a $BaTiO_3$/P(VDF-HFP) composite film and a PEI at 150 °C under a pressure of 6 MPa for 5 min. In this paper, the single layer $BaTiO_3$/P(VDF-HFP) composites and bilayer composites were denoted as α vol% BT/PVDF and PEI-α vol% BT/PVDF respectively, where α represents the volume fractions of $BaTiO_3$ in the $BaTiO_3$/P(VDF-HFP) composites.

View Article Online
DOI: 10.1039/D0TA00903B

2.3. Characterization and measurements

The morphologies of the bilayer films and elemental distributions of barium and carbon were observed by scanning electron microscopy (SEM, S-4800, Hitachi, Ltd.) coupled with EDX. Circular gold electrodes with a diameter of 2.98 mm were sputtered on the two sides of the samples before dielectric measurements. The dielectric properties were analyzed with an Agilent E4980A Precision LCR analyzer in the frequency range from 100 Hz to 1 MHz. Open and short compensations were performed before testing. The permittivity was calculated by $\varepsilon_r = tC_p/A\varepsilon_0$, where t is the thickness of the sample, A is the area of the electrode, C_p is the parallel capacitance, f is the electric field frequency, and ε_0 is the absolute permittivity of free space (8.85×10^{-12} F m^{-1}). The breakdown strengths were obtained using a setup equipped with a Treck 609A amplifier with a voltage ramping rate of 500 V/s at room temperature (PolyK Technologies, USA). The energy storage performances, including discharge energy densities and charge-discharge efficiencies were obtained by the *P-E* hysteresis loops which were collected at 1 kHz using a ferroelectric test system based on a modified Sawyer-Tower circuit (PolyK Technologies, USA).

3. Results and discussion

The optical photograph and cross-sectional SEM morphologies of the PEI-20 vol% BT/PVDF bilayer composite are presented in Figure 2a and 2b-d. As seen, the bilayer film is flexible and has smooth surfaces. The SEM image confirms the distinct bilayer configuration, in which the two layers are tightly welded together without the appearance of noticeable defects (e.g., pores, cracks, voids, etc.). Moreover, the high-

View Article Online
DOI: 10.1039/D0TA00903B

magnification cross-sectional SEM images shown in Figure S1 demonstrated that the $BaTiO_3$ particles are homogeneously dispersed in the P(VDF-HFP) matrix. The EDX mapping results further demonstrated that the $BaTiO_3$ particles are well restricted in the P(VDF-HFP) matrix without apparent diffusion into the PEI layer. Furthermore, the total thickness of the film is ~ 25 μm, where the BT/PVDF layer is ~ 6.6 μm while the PEI layer is ~ 18.4 μm. As we know, in a single-layer composite consisting of ferroelectric fillers (e.g., $BaTiO_3$) dispersed in a linear dielectric matrix (e.g., PEI, PMMA, PI), the ferroelectric fillers offer high energy-storage density while the matrix maintains the high energy-storage efficiency. As the loading fractions of ferroelectric fillers increases, the energy density increases and the efficiency decreases.[38,39] Similarly, in the bilayer-structured composites, the linear dielectric PEI layer is expected to contribute to the improved energy-storage efficiency, while the ferroelectric $BaTiO_3$/P(VDF-HFP) layer could suppress the efficiency because of its strong polarization-induced energy loss. Therefore, to achieve high efficiency, the volume fractions of ferroelectric $BaTiO_3$ and P(VDF-HFP) in the bilayer composites should be lowered. In this regard, the PEI layer is designed to be much thicker than the $BaTiO_3$/P(VDF-HFP) layer. However, it should be noted that the increasing thickness ratio of the PEI layer to the $BaTiO_3$/P(VDF-HFP) layer would also result in the suppressed energy-storage density. As shown in Figure S1, the thickness ratios of BT/PVDF layer to PEI layer for all the bilayer composites are almost the same, i.e., ~ 0.36. Accordingly, the volume ratio of the BT/PVDF layer to PEI layer is about 0.36, and the actual volume fractions of $BaTiO_3$ in the PEI-5 vol% BT/PVDF, PEI-10 vol% BT/PVDF, PEI-20 vol% BT/PVDF and PEI-40 vol% BT/PVDF composites are 1.8 %, 3.6 %, 7.2% and 14.4 %, respectively.

The frequency dependences of dielectric permittivity and loss tangent for single

View Article Online
DOI: 10.1039/D0TA00903B

layer and bilayer composites are displayed in Figure 3. As shown in Figure 3a, the pure PEI film shows the lowest permittivity and is almost independent of frequency in the tested frequency range. The pure P(VDF-HFP) has much higher permittivity than pure PEI and exhibits apparent frequency dispersion behavior. The permittivities of the $BaTiO_3$/P(VDF-HFP) composites increase with higher $BaTiO_3$ loadings, which could be attributed to the strong inherent dipolar polarization inside the ferroelectric $BaTiO_3$ particles. In addition, the interfacial polarization of the accumulated charges at the interfaces between $BaTiO_3$ particles and P(VDF-HFP) matrix may also contribute to the enhanced dielectric permittivity. Correspondingly, the pure PEI film possesses the lowest loss, while the pure PVDF and $BaTiO_3$/P(VDF-HFP) composites exhibit much higher loss than PEI (see Figure 3b). For instance, the loss tangents of the composites with 10 vol% and 20 vol% $BaTiO_3$ come up to above 0.1 @10 kHz, which may result in a huge amount of undesired heat production, thus deteriorating the performance stability and shortening the service life of the electronic devices. As shown in Figure 3c and 3d, the bilayer composites display moderate dielectric permittivities that are between the corresponding single layer $BaTiO_3$/P(VDF-HFP) composites and the pure PEI layer. Fortunately, low dielectric loss ($\tan\delta < 0.05$ @10 kHz) are achieved in the bilayer composites which will greatly facilitate their practical applications.

It should be noted that the magnitude of dielectric permittivity can only determine the energy density of a dielectric material under a certain electric field. In addition to permittivity, the maximum electric field that a dielectric material can withstand before failure (i.e., breakdown strength E_b) is another crucial parameter for dielectric energy-

View Article Online
DOI: 10.1039/D0TA00903B

storage materials, especially for the applications under high electric fields. Therefore, the breakdown strengths of the composites are further evaluated using the two-parameter Weibull distribution, which is described by Eq. (1):

$$P(E) = 1 - \exp\left[-\left(\frac{E}{\alpha}\right)^{\beta}\right] \quad (1)$$

where $P(E)$ is the cumulative failure probability, E is the experimentally tested breakdown electric field, α is the electric field for which there is a 63.2 % probability of sample breakdown (Weibull breakdown strength, E_b), and β is a shape parameter or the slope of the derived logarithm function reflecting the scatter of the tested E_b. When the β value is 3, the tested data follow Gaussian distribution, and a higher value of β implies a higher level of reliability. Figure 4 presents the Weibull E_b of the single layer and bilayer composites. We can see that, all of the plots show high β values, indicating high reliability of the measured data. The pure PEI has the highest E_b of ~ 607.35 kV/mm and pure P(VDF-HFP) also exhibits a high E_b of ~ 463.90 kV/mm. However, substantially deteriorated E_b, which are only ~ 35 %, ~ 29 %, 22 % and ~ 13 % of the pure P(VDF-HFP) matrix are observed in the single-layer BT/P(VDF-HFP) composites with 5 vol%, 10 vol%, 20 vol% and 40 vol% $BaTiO_3$, respectively. This is a widely reported phenomenon in ferroelectric ceramic/polymer composites because of the severe electric field distortion in the region near the ceramic particles which facilitates the development of electric trees.[27,30] It is worth noting that the bilayer composites show remarkably improved E_b compared with their single-layer counterparts. Specifically, the E_b of the bilayer composites with 5 vol%, 10 vol%, 20 vol% and 40 vol% $BaTiO_3$

View Article Online
DOI: 10.1039/D0TA00903B

are ~ 285 %, ~ 363 %, 366 % and ~ 567 % that of their single layer counterparts. In particular, the bilayer composite with 10 vol% $BaTiO_3$ exhibits an outstanding E_b of 483.18 kV/mm, which is even higher than that of the pure P(VDF-HFP). In the bilayer composites, although the BT/P(VDF-HFP) layer is easy to be broken down, the majority of the applied electric voltage will concentrate on the PEI layer which possesses high E_b, thus relieves the electric field in the BT/P(VDF-HFP) layer.[33-35] Moreover, the development of electric trees could be effectively blocked by the huge electric field gap between the two layers, thus preventing the electric trees from penetrating the entire bilayer composites. In addition, the electric trees may develop along the interfaces between the adjacent layers, yielding the increased length of electric tree development paths that is beneficial to the improvement of E_b.

The unipolar electric displacement-electric field (*P*-*E*) loops for the single layer and bilayer composites are illustrated in Figure 5, Figure S3 and Figure S4. Slim (or narrow) loops imply a weak deviation from the linear dielectric behavior and corresponds to a low energy loss. Clearly, the pure P(VDF-HFP) shows much wider loops than the pure PEI, and the introduction of $BaTiO_3$ particles further widens the loops, indicative of enhanced energy loss and suppressed efficiency (see Figure 5a). The bilayer composites possess slim loops located between the pure PEI and pure P(VDF-HFP), and no serious broadening phenomenon is observed in the loops under elevated electric fields (see Figure 5b and Figure S4). Figure 5c depicts the displacements of the pure PEI and bilayer composites with varied $BaTiO_3$ loading fractions at 350 kV/mm. As can be see, the bilayer composites exhibit substantially improved P_{max} (> 2 μC/cm^2) compared with the pure PEI (~ 1.25 μC/cm^2) which is

View Article Online
DOI: 10.1039/D0TA00903B

induced by the introduction of the ferroelectric BT/P(VDF-HFP) layer with strong dipolar and interfacial polarizations. In contrast, only slight increments of P_r (< 0.25 μC/cm^2) are observed, yielding the increased value of (P_{max}-P_r) which is beneficial to the concurrent improvement of energy density and efficiency. Moreover, the P_{max} of the composites get higher with increasing loading fractions of $BaTiO_3$ which should be ascribed to the high P_{max} (~ 0.085 C/m^2 at 3 kV/mm) of pure $BaTiO_3$ (see Figure S3b). Even though, higher $BaTiO_3$ content also brings about the enhanced deviations of *P-E* loops from linear behavior, leading to suppressed energy-storage performance. As can be seen in Figure S5, the PEI-40 vol% BT/PVDF composite shows higher P_{max} than the other bilayer composites with low $BaTiO_3$ contents under the same charging electric field. However, its breakdown strength is obviously lower than the other bilayer composites. Consequently, it can only be charged to 280 kV/mm and the corresponding efficiency is lower than that of the other bilayer composites. In a word, higher $BaTiO_3$ results in higher energy density but lower breakdown strength and lower efficiency. Furthermore, the stored energy densities (U_s) of the composites were derived from the *P-E* loops (see Figure 5(d, e) and Figure S3 and S4) by integration of the area between the charge curve and the ordinate, while the discharged energy densities (U_d) were obtained by integrating the area between the discharge curve and the ordinate, and the discharge efficiencies η were calculated using $\eta = U_d/U_s$. As illustrated in Figure 5e, although the single layer BT/P(VDF-HFP) composites show higher U_d than the corresponding bilayer composites at low electric fields (< 200 kV/mm) as a result of their high permittivities, they can not be used as energy storage materials under high electric fields owing to their low E_b as aforementioned. On the contrary, the bilayer composites display superior U_d under high electric fields and their energy densities are much higher than that of the pure PEI. Especially, a high energy density of ~ 6.0 J/cm^3

under an electric field of 450 kV/mm is achieved in the bilayer composite with 10 vol% $BaTiO_3$. The discharged efficiencies η of the composites under different electric fields are illustrated in Figure 5f. Apparently, ultrahigh η (> 95%) which are much higher than those of the single layer pure P(VDF-HFP) and BT/P(VDF-HFP) composites, are achieved. In the bilayer composites, the ultrahigh discharge efficiencies are mainly contributed by the introduction of the linear dielectric polymer PEI. On one hand, the aforementioned low volume fractions of ferroelectric phases, including $BaTiO_3$ and P(VDF-HFP), results in the low energy loss induced by ferroelectric polarizations, hence the high efficiency. On the other hand, the excellent insulating property of the PEI layer ensures the high breakdown strengths of the bilayer composites which can effectively suppress the ohmic heat loss induced by leakage conductance and deliver the high discharge efficiency. Furthermore, the ultrahigh η are well maintained even under high electric fields up to 450 kV/mm. In particular, the bilayer composite with 10 vol% $BaTiO_3$ exhibits an extremely high η of ~ 96.8 % at 450 kV/mm which is almost as high as that of the pure PEI (η ~ 98.2 %). In contrast, the η of the single-layer BT/P(VDF-HFP) composites become sharply deteriorated with increasing electric fields. As discussed above, the combination of linear and nonlinear dielectric polymers via constructing bilayer composites gives rise to comprehensively enhanced energy-storage performances.

Figure 6 compares the discharge efficiencies and energy densities of this work and recently reported single layer, bilayer, trilayer and multilayer (> 3 layers) polymer composites from other research groups. We can see that, the composites using linear dielectric polymer matrix (e.g., BNNS/PMMA composites in *Ref.* 46 and $BaTiO_3$/PI composites in *Ref.* 47) display relatively higher discharge efficiencies (> 80 %) than

View Article Online
DOI: 10.1039/D0TA00903B

those composites based on nonlinear dielectric polymers (e.g., PVDF and its copolymers). It is worth noting that, our bilayer PEI-10 vol% $BaTiO_3$/P(VDF-HFP) composite exhibits a much higher discharge efficiency (~ 96.8 %) than most of the so far reported polymer based dielectric composites. Meanwhile, a high energy density of ~ 6 J/cm^3 is also obtained. For a long time, the researches on dielectric energy-storage materials are mainly targeted at solely achieving high energy density. On the contrary, the discharged efficiency and loss that are key parameters in practical applications gained limited attention. The simultaneous realization of ultrahigh discharge efficiency along with high energy density, low loss, and high breakdown strength make these bilayer composites ideal candidates for applications in high-performances dielectric energy-storage devices.

4. Conclusion

In summary, a class of bilayer composites consisting of a pure polyetherimide layer and a $BaTiO_3$/P(VDF-HFP) composite layer were fabricated via solution casting and hot pressing. The bilayer composites show impressive improvements in breakdown strengths, i.e., 285 %, 363 %, 366% and 567 % for composites with 5 vol%, 10 vol%, 20 vol% and 40 vol% $BaTiO_3$ particles, in comparison with their single layer counterparts, thus results in obviously improved U_d. More notably, the bilayer composites exhibit ultrahigh discharged efficiencies over 95 %, which are much higher than most of the so far reported results, under external electric fields up to 400 kV/mm. Especially, the bilayer composite with 10 vol% $BaTiO_3$ exhibits an ultrahigh discharge efficiency of ~ 96.8 % and a high energy density of 6 J/cm^3 at 450 kV/mm, along with

View Article Online
DOI: 10.1039/D0TA00903B

a low loss tangent of ~ 0.025 @10 kHz. It is believed that, in the bilayer composites, the pure polyetherimide layer ensures high efficiency, high breakdown strength and low loss, while the $BaTiO_3$/P(VDF-HFP) composite layer offers high energy density. The synergy of the two layers brings about the concurrently enhanced discharge efficiency and energy density. The distinguished dielectric performances greatly promote the practical applications of these bilayer composites in advanced energy-storage devices. Hopefully, layer-structured composites with further improved dielectric properties may be developed via sufficiently exploring the synergic effects of the linear and nonlinear dielectric layers.

Acknowledgements

The authors acknowledge the financial support of this work by National Natural Science Foundation of China (51773187, 51402271), Foundation for Outstanding Young Scientist in Shandong Province (BS2014CL003).

References

1 X. Y. Huang, B. Sun, Y. K. Zhu, S. T. Li and P. K. Jiang, *Prog*. *Mater*. *Sci*., 2019, **100**, 187-225.

2 H. Luo, X. F. Zhou, C. Ellingford, Y. Zhang, S. Chen, K. C. Zhou, D. Zhang, C. R. Bowen and C.Y. Wang, *Chem*. *Soc*. *Rev*., 2019, **48**, 4424-4465.

3 H. Pan, F. Li, Y. Liu, Q. H. Zhang, M. Wang, S. Lan, Y. P. Zheng, J. Ma, L. Gu, Y. Shen, P. Yu, S. J. Zhang, L. Q. Chen, Y. H. Li and C.W. Nan, *Science*, 2019, **365**, 578-582.

4 Z. P. Li, X. Y. Chen, C. Zhang, E. Baer, D. Langhe, M. Ponting, M. Brubaker, T. Hosking, R. P. Li, M. Fukuto and L. Zhu, *ACS Appl*. *Polym*. *Mater*., 2019, **1**, 867-875.

5 Q. Y. Zhao, L. Yang, K. N. Chen, Y. Z. Ma, H. L. Ji, M. X. Shen, H. J. Huang, H. Y. He and J. H. Qiu, *Nano Energy*, 2019, **65**, 104007.

6 X. T. Zhu, J. Yang, D. Dastan, H. Garmestani, R. H. Fan and Z. C. Shi, *Compos*. *Pt*. *A-Appl*. *Sci*. *Manuf*., 2019, **125**, 105521.

7 J. Yang, X. T. Zhu, H. L. Wang, X. Wang, C. C. Hao, R. H. Fan, D. Dastan and Z. C. Shi, *Compos*. *Pt*. *A-Appl*. *Sci*. *Manuf*., 2020, **131**, 105814.

8 Y. N. Hao, X. H. Wang, K. Bi, J. M. Zhang, Y. H. Huang, L. W. Wu, P. Y. Zhao, K. Xu, M. Lei and L. T. Li, *Nano Energy*, 2017, **31**, 49-56.

9 C Zhang, Z. C. Shi, F. Mao, C. Q. Yang, J. Yang, X. T. Zhu and H Zuo, *J. Mater. Sci*, 2018, **53**, 1-13.

10 L. M. Yao, Z. B. Pan, J. W. Zhai, G. Z. Zhang, Z. Y. Liu and Y. H. Liu, *Compos*, *Pt*. *A-Appl*. *Sci*. *Manuf*., 2018, **109**, 48-54.

11 Z. B. Pan, B. H. Liu, J. W. Zhai, L. M. Yao, K. Yang and B. Shen, *Nano Energy*, 2017, **40**, 587-595.

12 Z. C. Shi, S. G. Chen, R. H. Fan, X. A. Wang, X. Wang, Z. D. Zhang and K. Sun, *J*. *Mater*. *Chem*. *C*, 2014, **2**, 6752.

13 X. Huang, X. Zhang, G. K. Ren, J. Y. Jiang, Z. K. Dan, Q. H. Zhang, X. Zhang, C.

View Article Online
DOI: 10.1039/D0TA00903B

W. Nan and Y. Shen, *J. Mater. Chem. A*, 2019, **7**, 15198.

14 P. T. Xie, Y. F. Li, Q. Hou, K. Y. Sui, C. Z. Liu, X. Y. Fu, J. X. Zhang, V. Murugadoss, J. C. Fan, Y. P. Wang, R.H Fan and Z.H Guo, *J. Mater. Chem. C*, 2020.

15 B. Xie, Y. W. Zhu, M. A. Marwat, S. J. Zhang, L. Zhang and H. B. Zhang, *J. Mater. Chem. A*, 2018, **6**, 20356.

16 W. Y. Li, Z. Q. Song, J. Qian, Z. Y. Tan, H. Y. Chu, X. Y. Wu, W. Nie and X. H. Ran, *Carbon*, 2019, **141**, 728-738.

17 K. Sun, J. N. Dong, Z. X. Wang, Z. Y. Wang, G. H. Fan, Q. Hou, L. Q. An, M. Y. Dong, R. H. Fan and Z. H. Guo, *J. Phys. Chem. C*, 2019, **123**, 23635-23642.

18 L. Zhang, Z. Liu, X. Lu, G. Yang, X. Y. Zhang and Z. Y. Cheng, *Nano Energy*, 2016, **26**, 550-557.

19 B. H. Fan, M. Y. Zhou, C. Zhang, D. L. He and J. B. Bai, *Prog. Polym. Sci.*, 2019, **97**, 101143.

20 M. F. Guo, J. Y. Jiang, Z. H. Shen, Y. H. Lin, C. W. Nan and Y. Shen, *Mater. Today*, 2019, **29**, 49-67.

21 K. Bi, M. H. Bi, Y. N. Hao, W. Luo, Z. M. Cai, X. H. Wang and Y. H. Huang, *Nano Energy*, 2018, **51**, 513-523.

22 G. Jian, M. R. Liu, C. Yan, F. Wu, B. Song, K. S. Moon and C. P. Wong, *Nano Energy*, 2019, **58**, 419-426.

View Article Online
DOI: 10.1039/D0TA00903B

23 M. S. Zheng, Y. T. Zheng, J. W. Zha, Y. Yang, P. Han, Y. Q. Wen and Z. M. Dang, *Nano Energy*, 2018, **48**, 144-151.

24 Y. Yang, Z. S. Gao, M. H. Yang, M. S. Zheng, D. R. Wang, J. W. Zha, Y. Q. Wen and Z. M. Dang, *Nano Energy*, 2019, **59**, 363-371.

25 Z. Y. Wang, K. Sun, P. T. Xie, Q. Hou, Y. Liu, Q. L. Gu and R. H. Fan, *Acta Mater*, 2020, **185**, 412-419.

26 Q. L. Fan, C. R. Ma, Y. Li, Z. S. Liang, S. Cheng, M. Y. Guo, Y. Z. Dai, C. S. Ma, L. Lu, W. Wang, L. H. Wang, X. J. Lou, M. Liu, H. Wang and C. L. Jia, *Nano Energy*, 2019, **62**, 725-733.

27 J. Y. Jiang, Z. H. Shen, J. F. Qian, Z. K. Dan, M. F. Guo, Y. He, Y. H. Lin, C. W. Nan, L. Q. Chen and Y Shen, *Nano Energy*, 2019, **62**, 220-229.

28 B. Xie, Q. Zhang, L. Zhang, Y. W. Zhu, X. Guo, P. Y. Fan and H. B. Zhang, *Nano Energy*, 2018, **54**, 437-446.

29 Z. X. Sun, C. R. Ma, M. Liu, J. Cui, L. Lu, J. B. Lu, X. J. Lou, L. Jin, H. Wang and C. L. Jia, *Adv*. *Mater*., 2017, **29**, 1604427.

30 Z. C. Shi, J. Wang, F. Mao, C. Q. Yang, C. Zhang and R. H. Fan, *J*. *Mater*. *Chem*. *A*, 2017, **5**, 14575.

31 J Wang, Z. C. Shi, F. Mao, S. G. Chen and X. Wang, *ACS Appl*. *Mater*. *Interfaces*, 2017, **9**, 1793-1800.

32 J. Chen, Y. F. Wang, X. W. Xu, Q. B. Yuan, Y. J. Niu, Q. Wang and H. Wang, *J. Mater. Chem. A*, 2019, **7**, 3729.

33 Y. F. Wang, L. X. Wang, Q. B. Yuan, J. Chen, Y. J. Niu, X. W. Xu, Y. T. Cheng, B. Yao, Q. Wang and H. Wang, *Nano Energy*, 2018, **44**, 364-370.

34 C. Jie, Y. F. Wang, Q. B. Yuan, X. W. Xu, Y. J. Niu, Q. Wang and H. Wang, *Nano Energy* 2018, **54**, 288-296.

35 Y. F. Wang, J. Chen, Y. Li, Y. J. Niu, Q. Wang and H. Wang, *J. Mater. Chem. A*, 2019, **7**, 2965.

36 Y. F. Wang, Y. Li, L. X. Wang, Q. B. Yuan, J. Chen, Y. J. Niu, X. W. Xu, Q. Wang and H. Wang, *Energy Storage Mater.*, 2020, **24**, 626-634.

37 C. Zhang, Z. C. Shi, F. Mao, C. Q. Yang, X. T. Zhu, J. Yang, H. Zuo and R. H. Fan, *ACS Appl. Mater. Interfaces*, 2018, **10**, 26713-26722.

38 Y. Feng, Y. H. Zhou, T. D. Zhang, C. H. Zhang, Y. Q. Zhang, Y. Zhang, Q. G. Chen and Q. G. Chi, *Energy Storage Mater.*, 2020, **25**, 180-192.

39 Y. Zhang, C. H. Zhang, Y. Feng, T. D. Zhang, Q. G. Chen, Q. G. Chi, L. Z. Liu, X. Wang and Q.Q. Lei, *Nano Energy*, 2019,**64**, 104195.

40 D. Zhang, W. W. Liu, R. Guo, K. C. Zhou and H. Luo, *Adv. Sci.*, 2018, **5**, 1700512.

41 H. J. Ye, T. M. Lu, C. F. Xu, M. Q. Zhong and L. X. Xu, *Nanotechnology*, 2018, **29**, 095702.

View Article Online
DOI: 10.1039/D0TA00903B

42 H. J. Ye, X. H. Zhang, C. F. Xu, B. Han and L. X. Xu, *J. Mater. Chem. C*, 2018, **6**, 11144-11155.

43 Z. B. Pan, L. M. Yao, J. W. Zhai, H. T. Wang and B. Shen, *ACS Appl. Mater. Interfaces*, 2017, **9**, 14337-14346.

44 L. Wang, H. Luo, X. F. Zhou, X. Yuan, K. C. Zhou and D. Zhang, *Compos. Pt. A-Appl. Sci. Manuf.*, 2019, **117**, 369-376.

45 M. A. Marwat, B. Xie, Y. W. Zhu, P. Y. Fan, W. G. Ma, H. M. Liu, M. Ashtar, J. Z. Xiao, D. Salamon, C. Samater and H. B. Zhang, *Compos. Pt. A-Appl. Sci. Manuf.*, 2019, **121**, 115-122.

46 F. H. Liu, Q. Li, Z. Y. Li, Y. Liu, L. J. Dong, C. X. Xiong and Q. Wang, *Compos. Sci. Technol.*, 2017, **142**, 139-144.

47 W. D. Sun, X. J. Lu, J. Y. Jiang, X. Zhang, P. H. Hu, M. Li, Y. H. Lin, C. W. Nan and Y. Shen, *J. Appl. Phys.* 2017, **121**, 244101.

48 Q. G. Chi, X. B. Wang, C. H. Zhang, Q. G. Chen, M. H. Chen, T. D. Zhang, L. Gao, Y. Zhang, Y. Cui, X. Wang and Q. Q. Lei, *ACS Sustain. Chem. Eng.*, 2018, **6**, 8641-8649.

49 Y. Zhang, T. D. Zhang, L. Z. Liu, Q. G. Chi, C. H. Zhang, Q. G. Chen, Y. Cui, X. Wang and Q. Q. Lei, *J. Phys. Chem. C*, 2018, **122**, 1500-1512.

50 W. Y. Li, Z. Q. Song, J. M. Zhong, J. Qian, Z. Y. Tan, X. Y. Wu, H. Y. Chu, W. Nie and X. H. Ran, *J. Mater. Chem. C*, 2019, **7**, 10371.

View Article Online
DOI: 10.1039/D0TA00903B

51 M. A. Marwat, B. Xie, Y. W. Zhu, P. Y. Fan, K. Liu, M. Shen, M. Ashtar, S. Kongparakul, C. Samater and H. B. Zhang, *Colloid Surf. A-Physicochem. Eng. Asp.*, 2019, **581**, 123802.

Figures

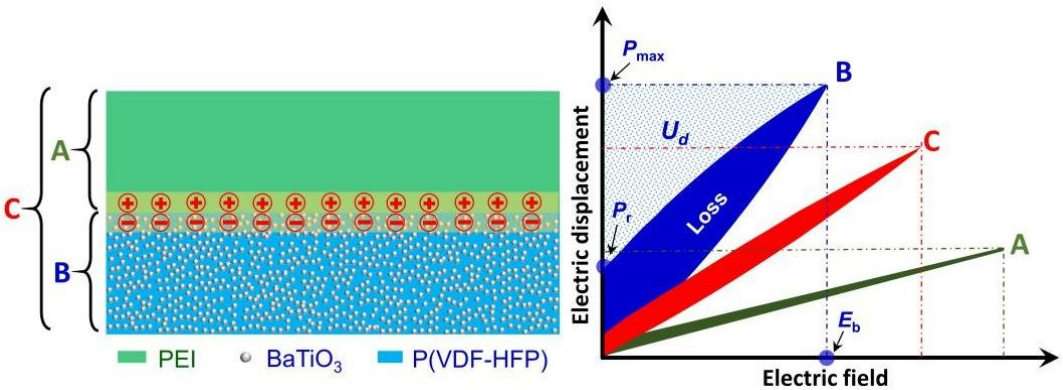

	Material	Dielectric behavior	U_d	η	Loss	E_b
A	Pure PEI	Linear	Low	★ High	★ Low	★ High
B	$BaTiO_3$/P(VDF-HFP)	Nonlinear	★ High	Low	High	Low
C	Bilayer PEI-$BaTiO_3$/P(VDF-HFP)	Linear-Nonlinear	★ High	★ High	★ Low	★ High

Fig. 1 Schematic illustration of the dielectric energy-storage characteristics of linear dielectric, nonlinear dielectric and bilayer linear/nonlinear dielectric composites. The pentagrams indicate the desired properties.

View Article Online
DOI: 10.1039/D0TA00903B

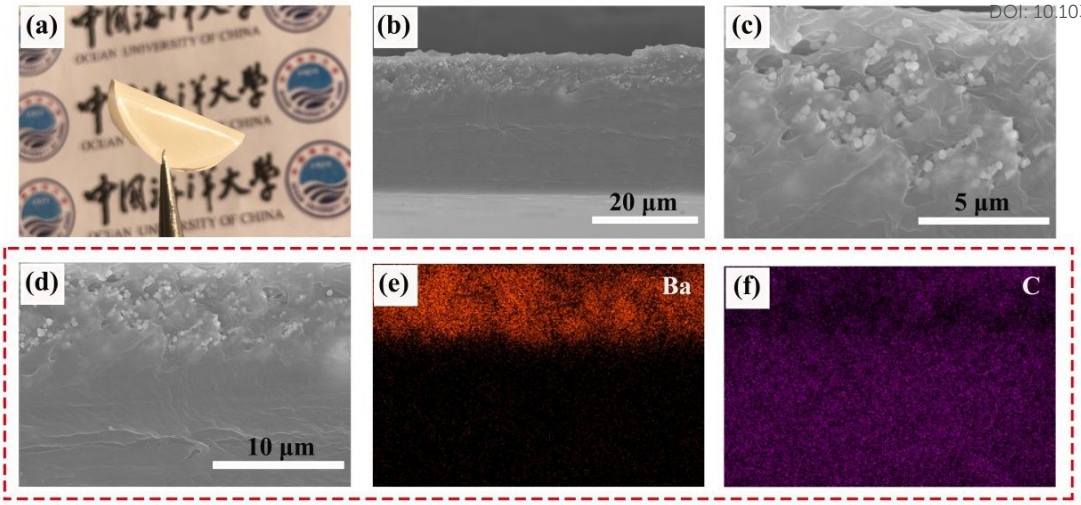

Fig. 2 (a) Photograph, (b-d) cross-sectional SEM morphologies and (e, f) corresponding EDX mapping images of the PEI-20 vol% BT/PVDF bilayer composite.

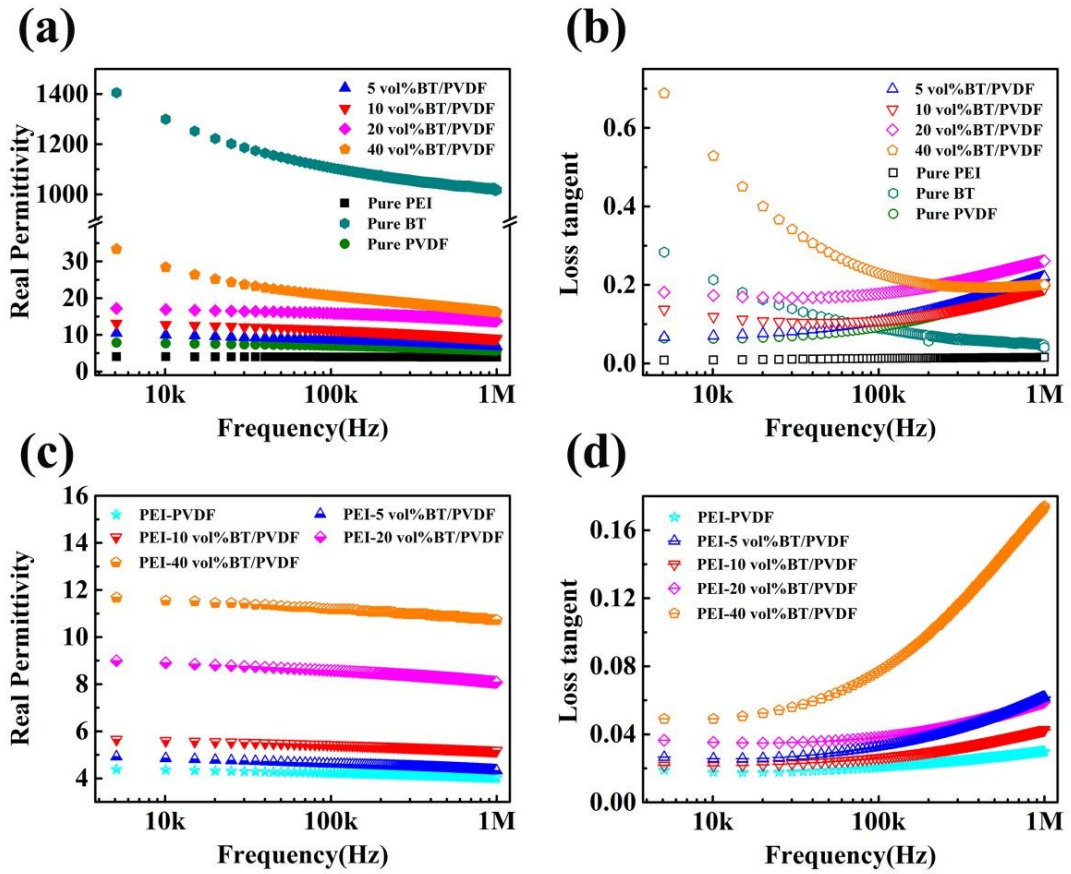

View Article Online
DOI: 10.1039/D0TA00903B

Fig. 3 Frequency dependences of dielectric permittivity and loss tangent for (a, b) single layer and (c, d) bilayer composites.

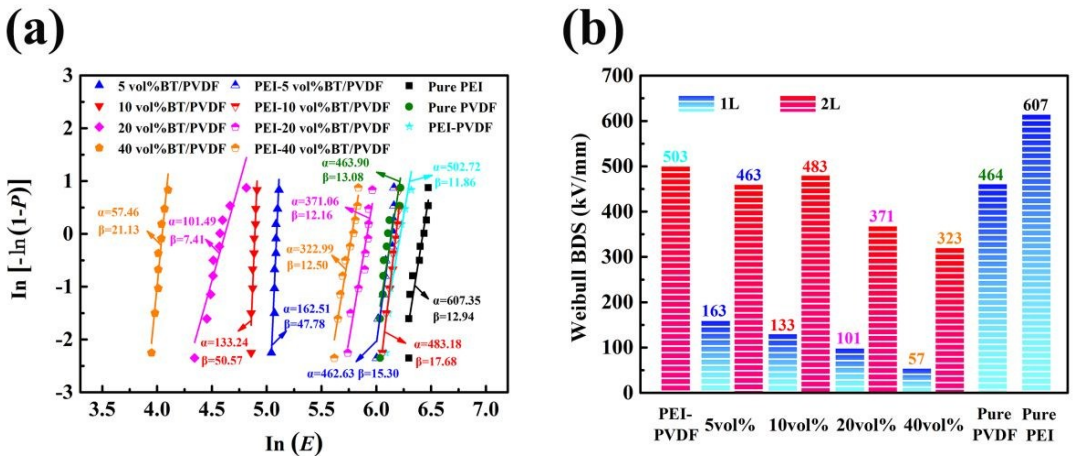

Fig. 4 (a) Weibull distribution plots, (b) characteristic breakdown strengths of the single layer and bilayer composites with different $BaTiO_3$ loading fractions.

View Article Online
DOI: 10.1039/D0TA00903B

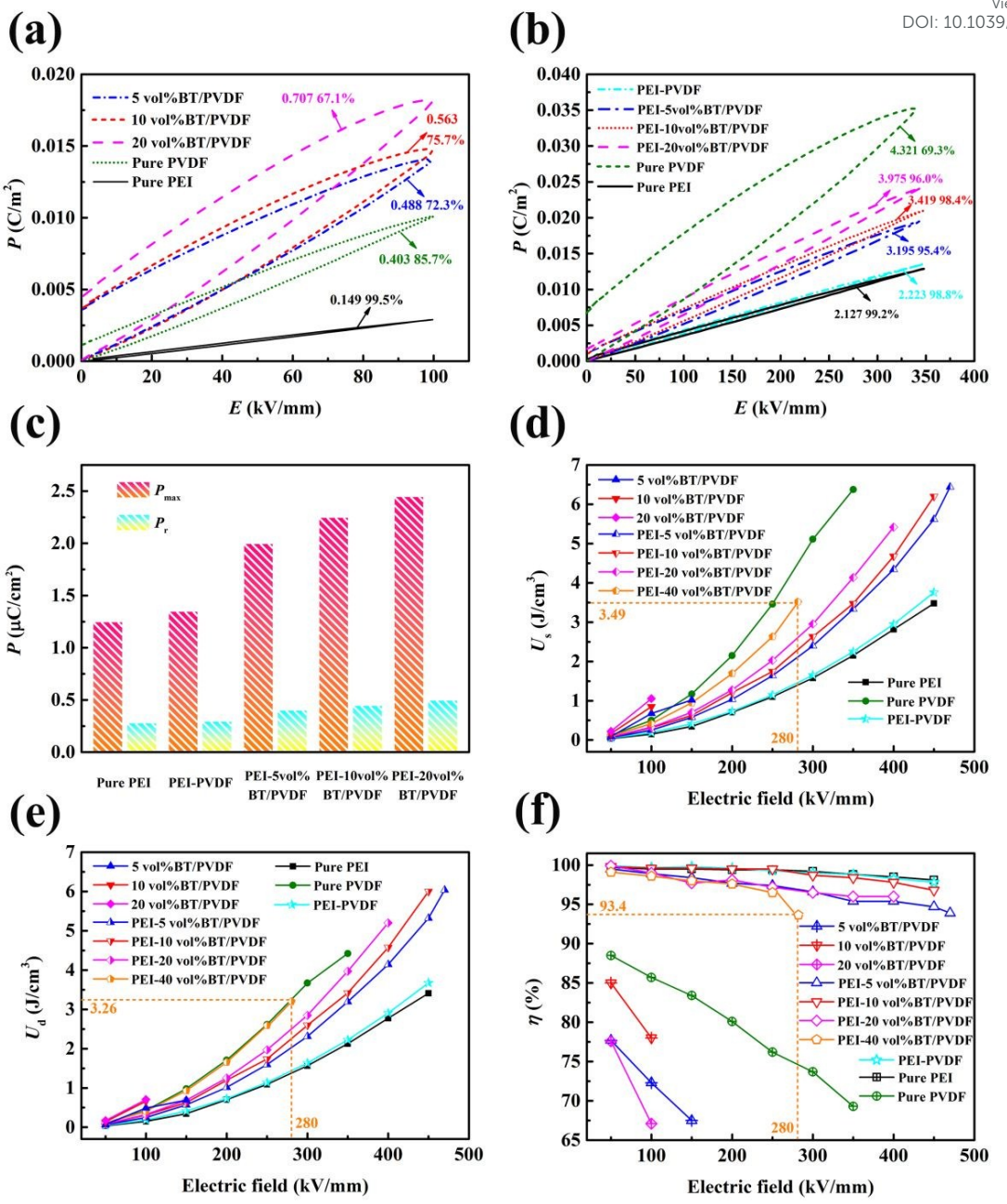

Fig. 5 *P*-*E* loops of (a) single layer composites and (b) bilayer composites with different $BaTiO_3$ loadings. (c) The maximum displacement P_{max} and remnant displacement P_r of the pure PEI and bilayer composites at 350 kV/mm. (d) The storage energy densities, (e) discharged energy densities and (f) discharged efficiencies of the single layer and bilayer composites under varied external electric fields.

View Article Online
DOI: 10.1039/D0TA00903B

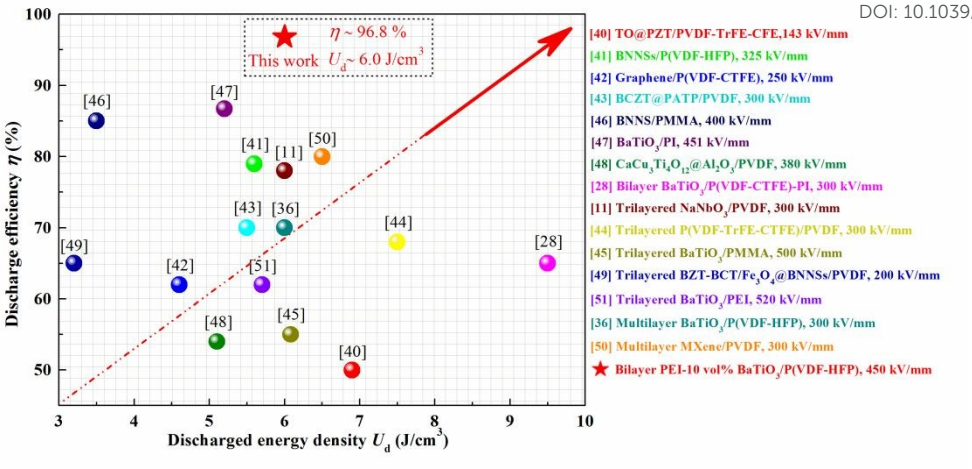

Fig. 6 Comparison of energy density and efficiency of this work (PEI-10 vol%$BaTiO_3$/P(VDF-HFP) composite) and reported results.